



*Journal of Geophysical Research: Earth Surface*

Supporting Information for

**The role of lithospheric flexure in the landscape evolution of the Wilkes Subglacial Basin  
and Transantarctic Mountains, East Antarctica**

Guy J. G. Paxman<sup>1</sup>, Stewart S. R. Jamieson<sup>1</sup>, Fausto Ferraccioli<sup>2</sup>, Michael J. Bentley<sup>1</sup>, Neil Ross<sup>3</sup>, Anthony B. Watts<sup>4</sup>, German Leitchenkov<sup>5,6</sup>, Egidio Armadillo<sup>7</sup>, Duncan A. Young<sup>8</sup>

<sup>1</sup> Department of Geography, Durham University, Durham, UK

<sup>2</sup> British Antarctic Survey, Cambridge, UK

<sup>3</sup> School of Geography, Politics and Sociology, Newcastle University, Newcastle upon Tyne, UK

<sup>4</sup> Department of Earth Sciences, Oxford University, Oxford, UK

<sup>5</sup> Institute for Geology and Mineral Resources of the World Ocean, St. Petersburg, Russia

<sup>6</sup> St. Petersburg State University, St. Petersburg, Russia

<sup>7</sup> Dipartimento di Scienze della Terra, dell'Ambiente e della Vita, Università di Genova, Genova, Italy

<sup>8</sup> University of Texas Institute for Geophysics, Austin, Texas, USA

**Table of Contents**

This file (2018JF004705\_SOM01.pdf)

Accompanying dataset (2018JF004705\_SOM02.zip)

**Contents of this file**

Figures S1 to S9

**Introduction**

This document contains details of the bedrock elevation data compilation (Figure S1), sensitivity testing for the 3D flexural modeling (Figure S2, S3, S4), 2D flexural modeling (Figure S5, S6), and changes in regional bedrock topography between the Eocene–Oligocene Boundary and the present-day, along with the associated uncertainties (Figure S7, S8, S9).

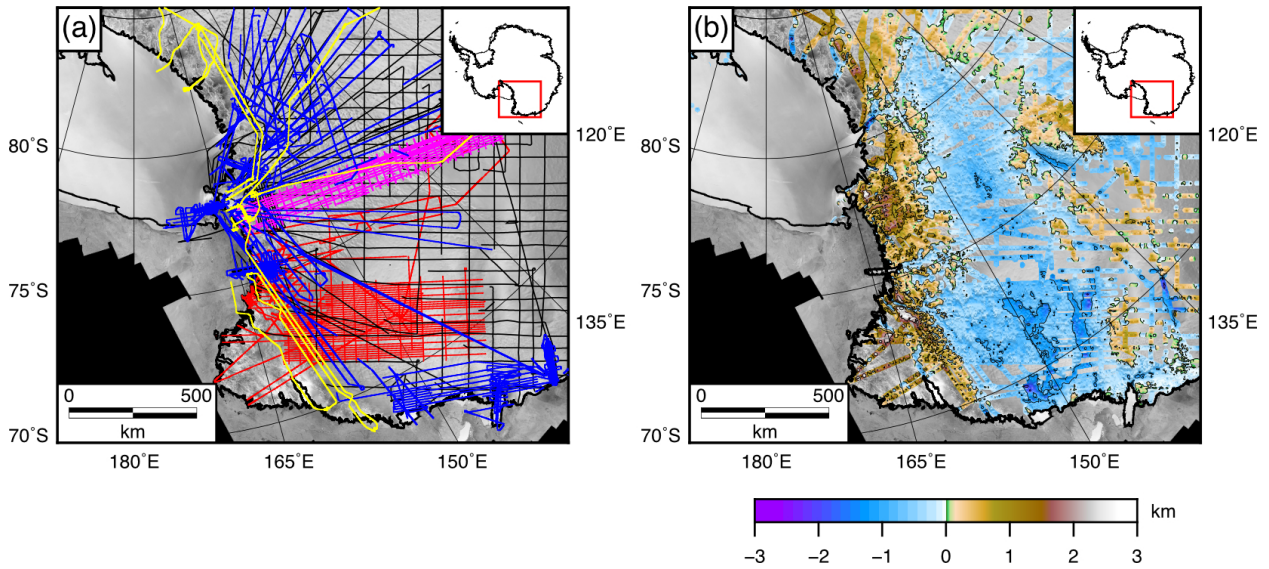


**Fig. S1.** Compilation of airborne radio-echo sounding (RES) datasets over the Transantarctic Mountains and Wilkes Subglacial Basin. (a) Airborne radar survey airborne flight coverage. The aircraft flight paths for the WISE-ISODYN (red), ICECAP (blue), Operation IceBridge (yellow), AEROTAM (magenta), and SPRI-NSF-TUD consortium (black) surveys are displayed. (b) New compilation of bedrock topography derived from the RES surveys shown in panel a. Points in the digital elevation model >10 km from the nearest raw data point have been masked. Contour interval is 1000 m and elevations are relative to mean sea level. For our complete grids in the main manuscript, offshore bathymetry data were taken from Bedmap2 (Fretwell et al., 2013), as were onshore bedrock topography data in regions of poor RES coverage (i.e. the masked regions in panel b).

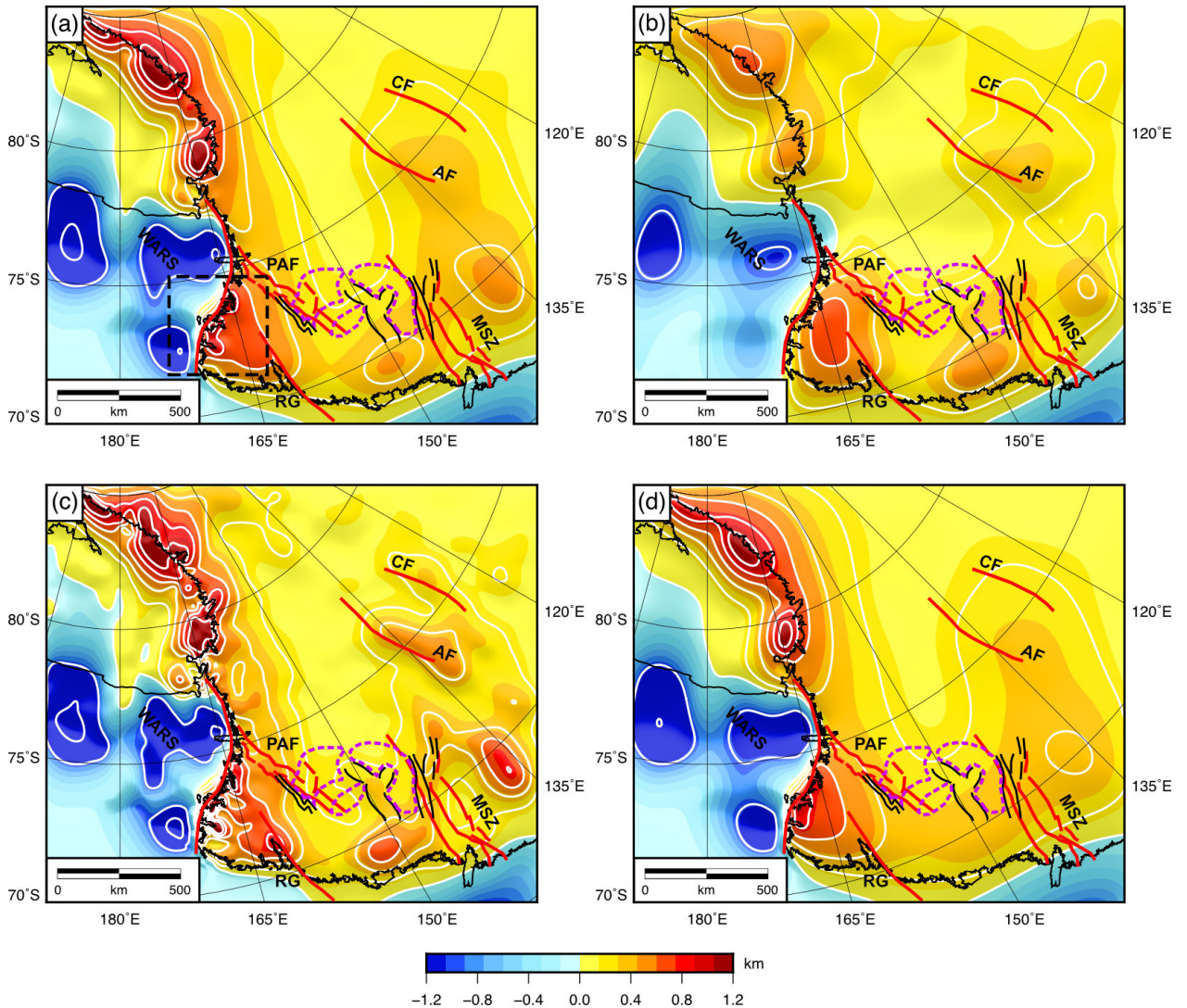


**Fig. S2.** Sensitivity testing to determine the influence of the elastic thickness on flexure in the Transantarctic Mountains (TAM) and Wilkes Subglacial Basin (WSB). (a) Flexural response to incisional unloading (warm colors) and sediment loading (cool colors) since 34 Ma for the  $T_e$  scenario described in the main manuscript, varying from 5 km at the front of the TAM to 50 km across the WSB. Contour interval is 0.2 km onshore and 1 km offshore. Dashed box shows the outline of the region covered in Fig. S3. (b) Flexural response for a spatially constant  $T_e$  value of 35 km (Wilson et al., 2012). (c) Flexural response for a scenario where  $T_e$  varies from 5 km at the front of the TAM to 20 km across the WSB. (d) Flexural response for a scenario where  $T_e$  varies from 5 km at the front of the TAM to 80 km across the WSB. The variation in the calculated flexural uplift between these end-member scenarios is <200 m in the WSB and <400 m along the TAM. Red lines are major crustal faults (Aitken et al., 2014; Cianfarra and Salvini, 2016; Ferraccioli and Bozzo, 2003); black lines show sub-basin outlines (Ferraccioli et al., 2009); dashed magenta lines mark the extent of flat bedrock plateaus (Paxman et al., 2018). Abbreviations of major fault systems: AF = Adventure Fault; CF = Concordia Fault; MSZ = Mertz Shear Zone; PAF = Prince Albert Fault; RG = Rennick Graben; WARS = West Antarctic Rift System.

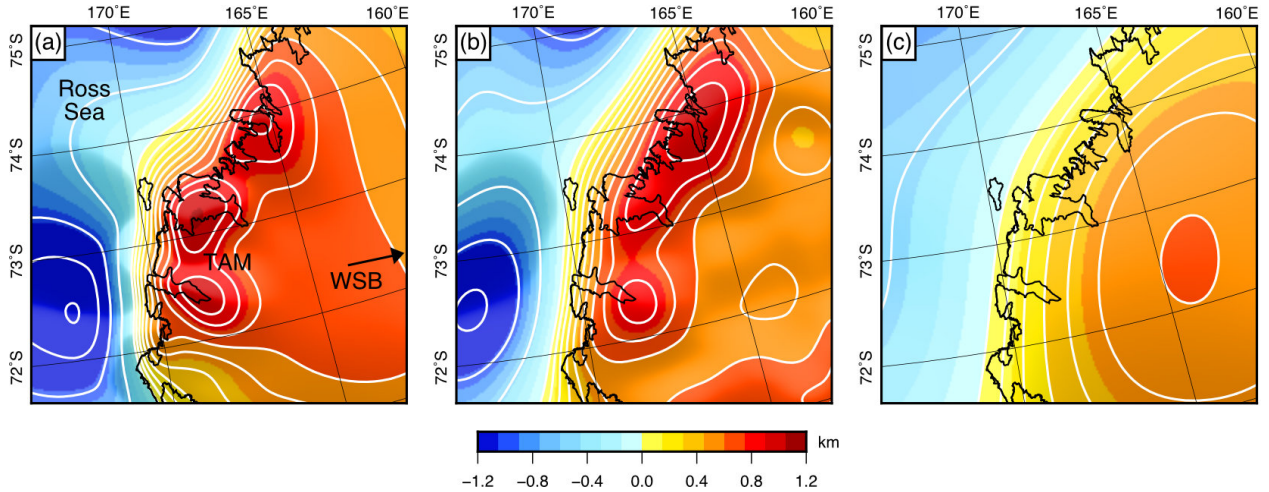


**Fig. S3.** Bench testing the numerical computation of flexural uplift for an elastic plate with a spatially variable elastic thickness. Panel location covers Victoria Land in the northern TAM and is shown in Fig. S2. (a) Flexural response to incisional unloading (warm colors) and sediment loading (cool colors) since 34 Ma for the  $T_e$  scenario described in the main manuscript, varying from 5 km at the front of the TAM to 50 km across the WSB. Contour interval is 0.1 km onshore and 0.5 km offshore. The flexure in this model is computed numerically using a centered finite difference approach. (b) Flexural response for a spatially constant  $T_e$  value of 10 km, approximately corresponding to the values assumed for the Ross Sea and edge of the TAM (see Fig. 2 in the main manuscript). (c) Flexural response for a spatially constant  $T_e$  value of 50 km, corresponding to the values assumed for the WSB (see Fig. 2 in the main manuscript). The flexure in panels b and c was computed analytically using a fast Fourier Transform method (Watts, 2001). The flexure in panel a closely approximates the low (10 km)  $T_e$  scenario in the Ross Sea and along the front of the TAM, and then approaches the high  $T_e$  scenario into the hinterland of the TAM and the WSB, indicating that the numerical solution is performing as expected.

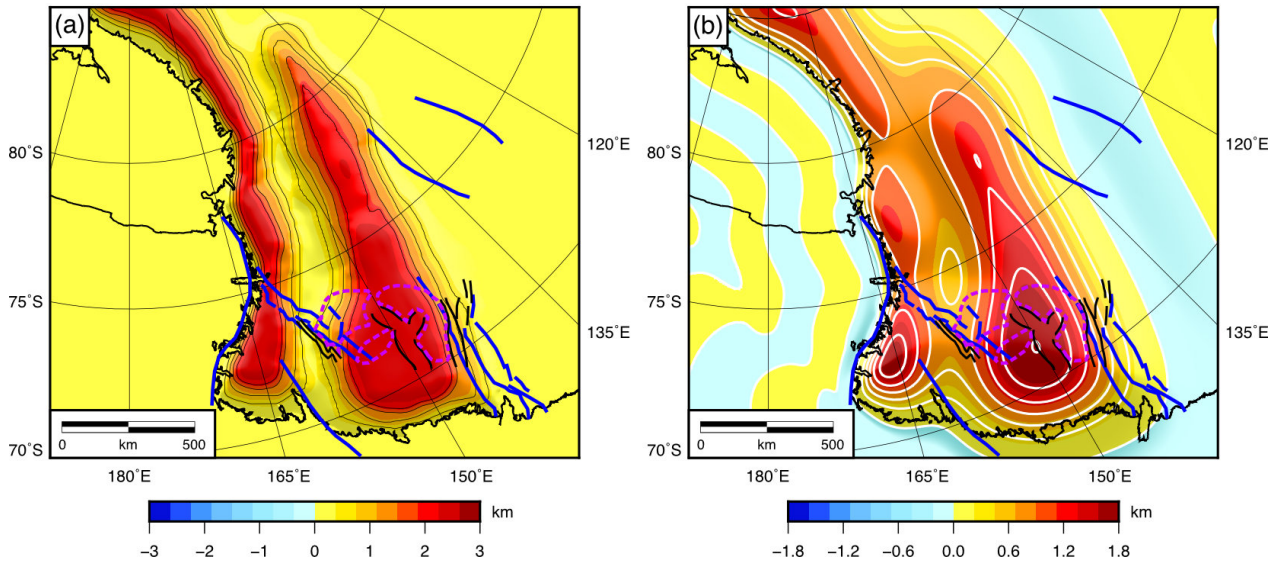


**Fig. S4.** Downwearing of post-Ferrar (ca. 180–35 Ma) sediments and the associated flexural response. (a) Assumed thickness of the ‘Mesozoic Victoria Basin’ (Prenzel et al., 2018). The sediment thickness grid is derived from thermochronological and geophysical data (Prenzel et al., 2018), but is largely qualitative in nature. Contour interval is 0.5 km. These basin deposits are assumed to have been rapidly removed by erosional downwearing in the Late Eocene / Early Oligocene (Lisker and Läufer, 2013; Prenzel et al., 2018). The total basin volume is  $1.7 \times 10^6 \text{ km}^3$ , which corresponds to a mass of 3.90 Pg assuming a sediment density of  $2350 \text{ kg m}^{-3}$ . (b) Flexural response to the removal of the sediment load in panel a using our standard scenario where  $T_e$  varies from 5 km at the front of the TAM to 50 km across the WSB. Contour interval is 0.3 km. Blue lines are major crustal faults (Aitken et al., 2014; Cianfarra and Salvini, 2016; Ferraccioli and Bozzo, 2003); black lines show sub-basin outlines (Ferraccioli et al., 2009); dashed magenta lines mark the extent of flat bedrock plateaus (Paxman et al., 2018).

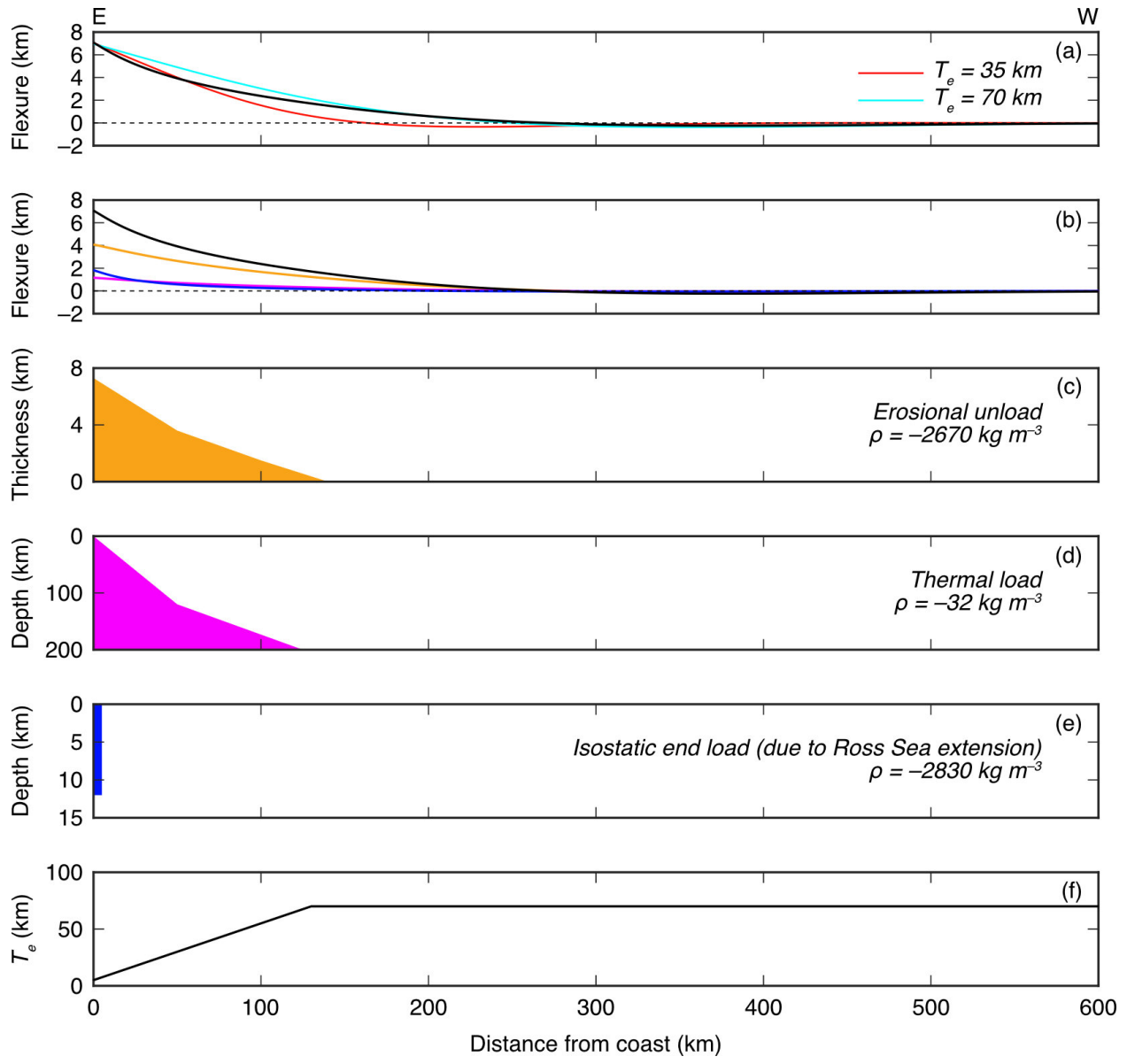


**Fig. S5.** Geometry of the loads and elastic thickness used in our 2D models of TAM uplift. Load geometries follow those of ten Brink et al. (1997). (a) Comparison between flexure computed using a spatially variable  $T_e$  model (panel f) with a plate break along the front of the TAM (black line) (ten Brink et al., 1997) and an analytical solution for a rectangular load on the end of a semi-infinite beam using Hetényi functions (Watts, 2001) for two constant  $T_e$  values. This shows that the variable  $T_e$  model performs as expected along the profile. (b) Flexure profiles. The black line represents the total flexural uplift, which is the sum of three components arising from separate driving loads (these lines are colored to match the corresponding loads in panels c, d and e). (c) Erosional unload due to the removal of a 'wedge' of material at the front of the TAM. An upper crustal density of  $2670 \text{ kg m}^{-3}$  is used for the eroded material. (d) Thermal load arising from lateral heat conduction from West Antarctica to East Antarctica. (e) Isostatic end load which represents mechanical unloading due to extension in the Ross Sea. Densities are given as negative values to reflect the fact that each 'load' is buoyant (acts upwards) and therefore drives surface uplift. (f) Variation in elastic thickness ( $T_e$ ) from the coast into the interior of East Antarctica, following ten Brink et al. (1997).

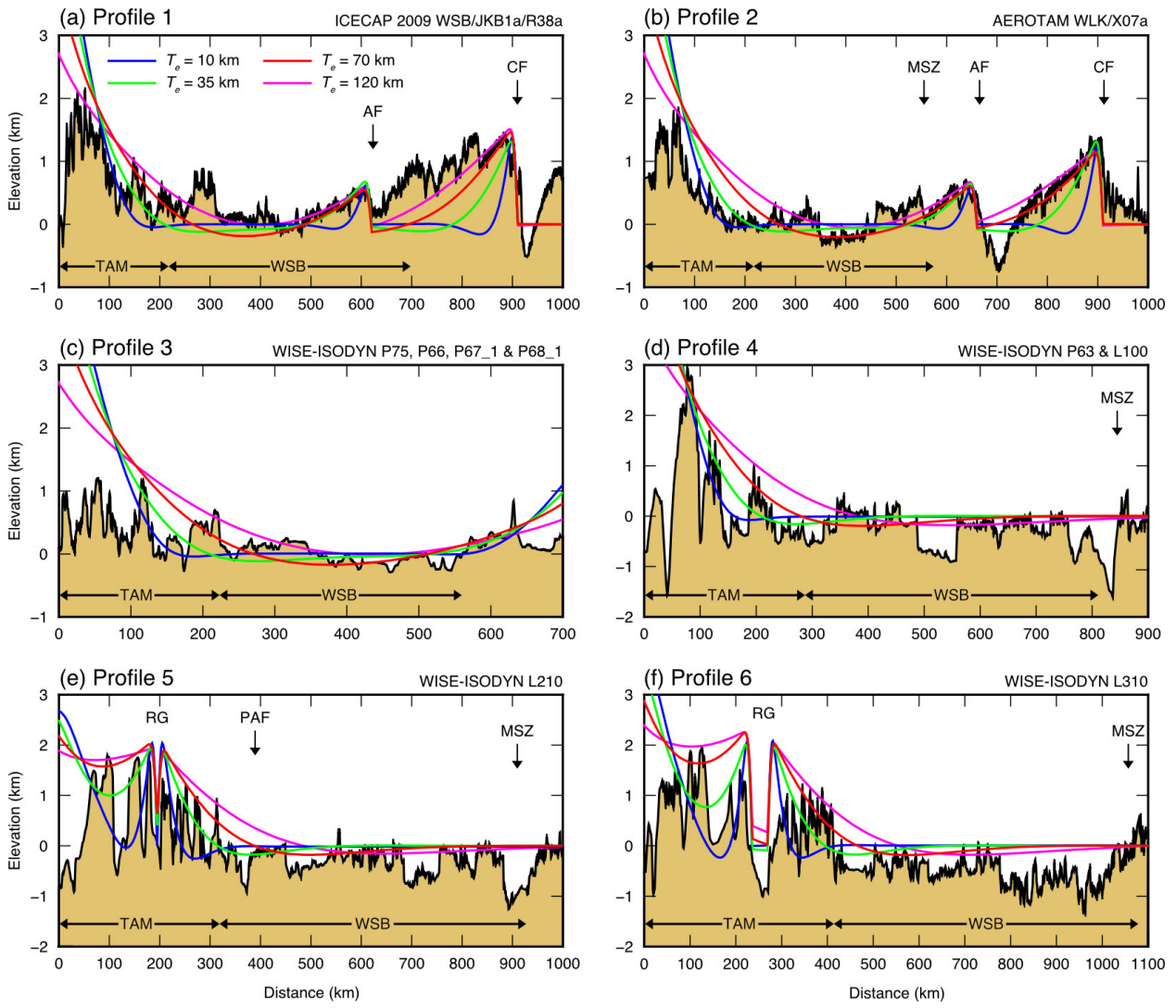


**Fig. S6.** Effect of  $T_e$  variations within the Wilkes Subglacial Basin. 2D flexural models along six radar profiles crossing the Transantarctic Mountains (TAM) and Wilkes Subglacial Basin (WSB). Profile locations (1–6, shown in panels a–f) are displayed in Fig. 5d and Fig. 7a in the main manuscript. RES lines were obtained from the ICECAP (1), AEROTAM (2), and WISE-ISODYN (3–6) surveys. The names of the lines, as given in the individual geophysical surveys, are provided. The bedrock is shown by the black line and shaded region. Bed elevations have been adjusted for the effects of ice sheet loading, incisional unloading, and sediment loading. Colored lines show the modelled topography for different  $T_e$  models.  $T_e$  is assumed to increase from 5 km at the eastern edge of the TAM (left edge of profiles) (following ten Brink et al., 1997), to a constant higher value beneath the WSB. We experimented by varying the higher value of  $T_e$  between 10 and 120 km. Lower  $T_e$  values (10–35 km) produce a better fit for the western TAM and eastern WSB, whereas higher  $T_e$  values (~70 km) give a closer match in the western WSB, indicating that  $T_e$  gradually increases westwards across the basin. Abbreviations of major faults: AF = Adventure Fault; CF = Concordia Fault; MSZ = Mertz Shear Zone; PAF = Prince Albert Fault; RG = Rennick Graben.

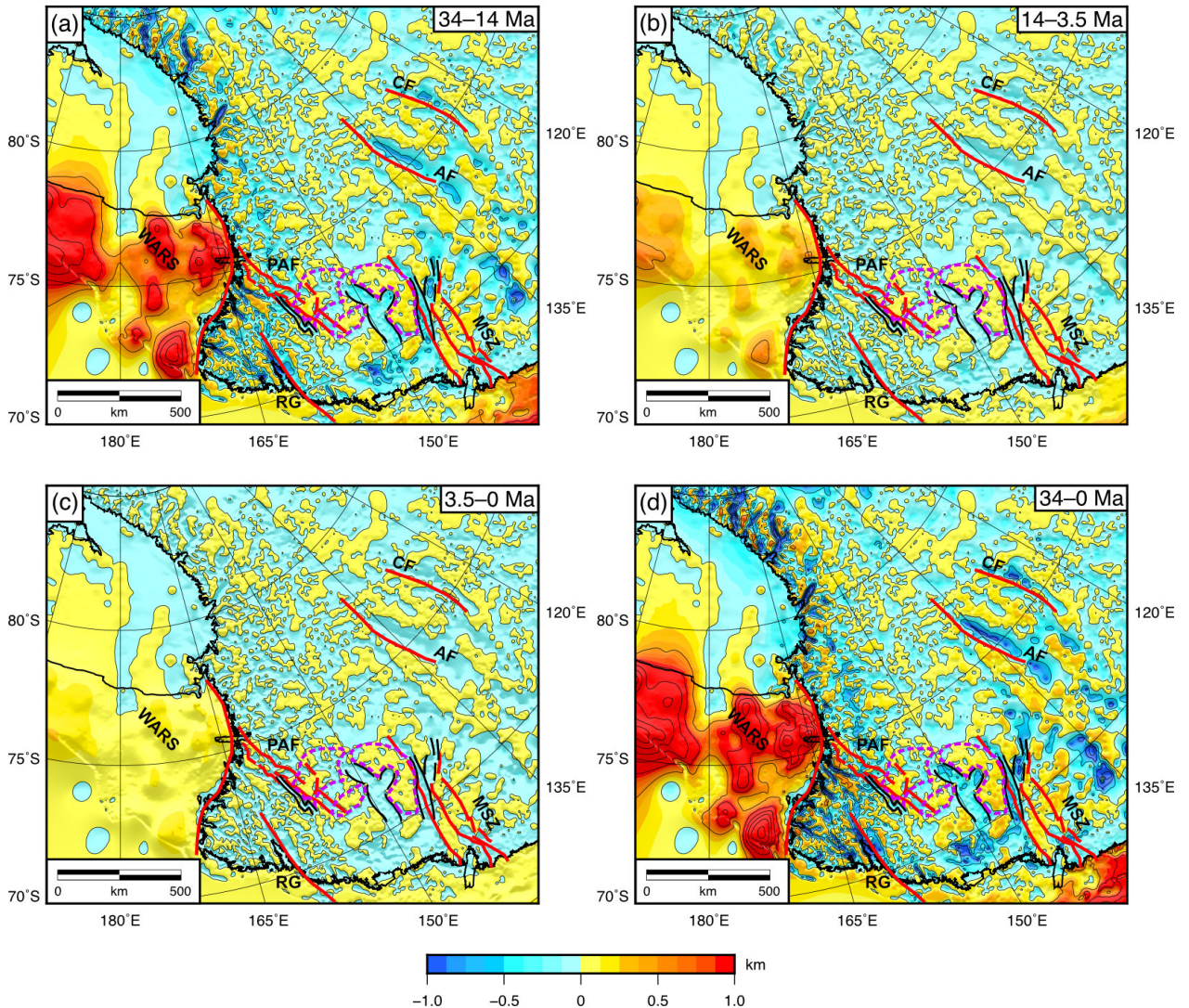


**Fig. S7.** Changes in the bedrock elevation of the Transantarctic Mountains and Wilkes Subglacial Basin since 34 Ma. (a) Change in bedrock topography between the Eocene–Oligocene Boundary (34 Ma) and the mid-Miocene (14 Ma). Warm colors denote positive surface displacement (e.g. due to uplift or sedimentation); cool colors denote negative surface displacement (e.g. due to subsidence or erosion). Contour interval is 500 meters. (b) Change in bedrock topography between the mid-Miocene (14 Ma) and mid-Pliocene (3.5 Ma). (c) Change in bedrock topography between the mid-Pliocene (14 Ma) and the present-day (0 Ma). (d) Total change in bedrock elevation from EAIS inception at ca. 34 Ma to present (excluding isostatic subsidence due to ice loading). Red lines are major crustal faults (Aitken et al., 2014; Cianfarra and Salvini, 2016; Ferraccioli and Bozzo, 2003); black lines show sub-basin outlines (Ferraccioli et al., 2009); dashed magenta lines mark the extent of flat bedrock plateaus (Paxman et al., 2018). Abbreviations of major fault systems: AF = Adventure Fault; CF = Concordia Fault; MSZ = Mertz Shear Zone; PAF = Prince Albert Fault; RG = Rennick Graben; WARS = West Antarctic Rift System.

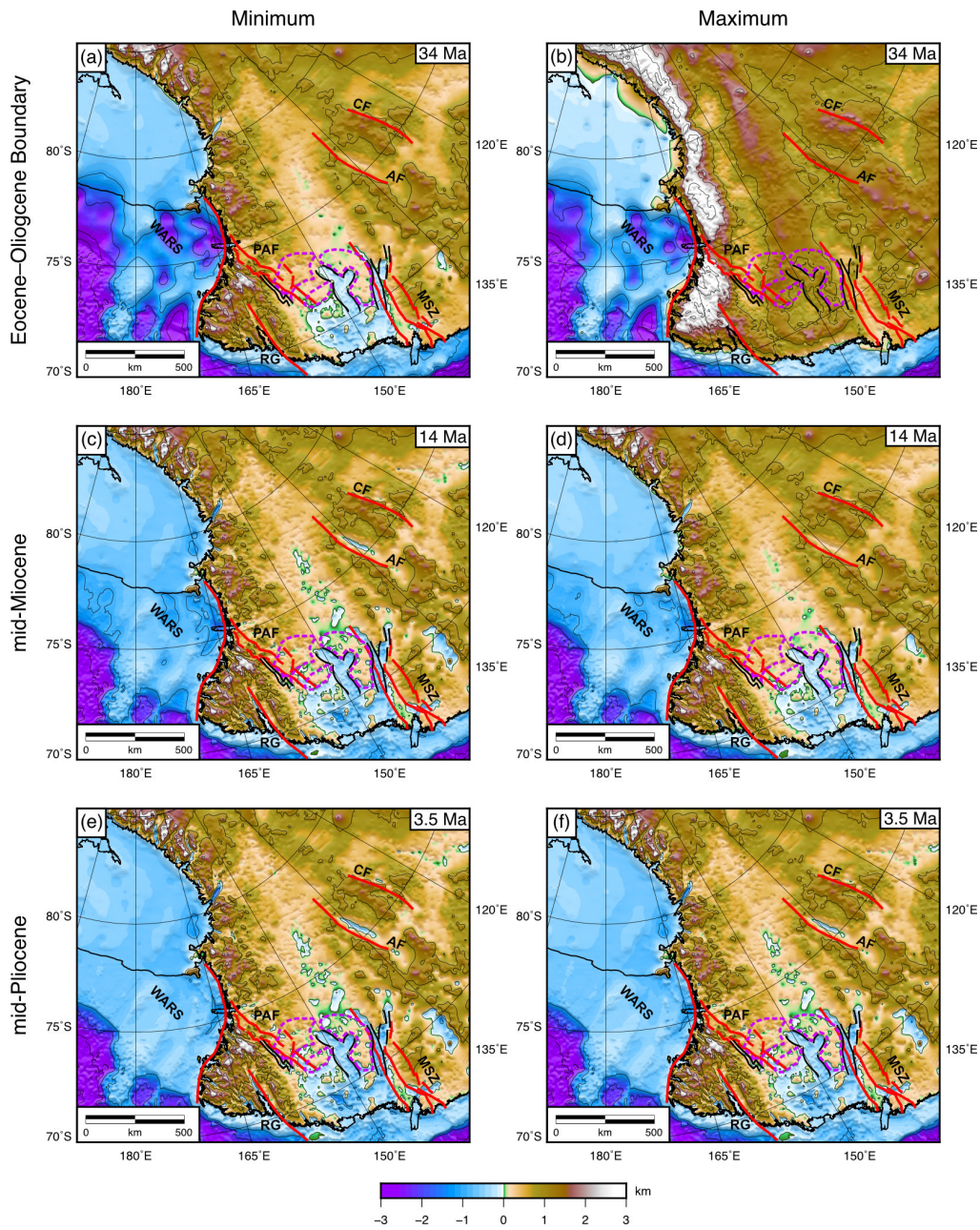


**Fig. S8.** Minimum and maximum reconstructed topography maps. Paleotopography maps are shown for the Eocene–Oligocene Boundary (ca. 34 Ma; panels a and b), the mid-Miocene (ca. 14 Ma; panels c and d), and the mid-Pliocene (ca. 3.5 Ma; panels e and f). Contour interval is 500 meters. The estimated eroded thicknesses (and associated flexure) for the minimum and maximum topographies are 50% lower and higher than the average estimate (Fig. 3 in the main manuscript), respectively. The maximum ca. 34 Ma topography also incorporates a correction for the downwearing of the ‘Mesozoic Victoria Basin’ (Fig. S4). Red lines are major crustal faults (Aitken et al., 2014; Cianfarra and Salvini, 2016; Ferraccioli and Bozzo, 2003); black lines show sub-basin outlines (Ferraccioli et al., 2009); dashed magenta lines mark the extent of flat bedrock plateaus (Paxman et al., 2018). Abbreviations of major fault systems: AF = Adventure Fault; CF = Concordia Fault; MSZ = Mertz Shear Zone; PAF = Prince Albert Fault; RG = Rennick Graben; WARS = West Antarctic Rift System. The minimum and maximum topographies for each time slice are available to download in the supplementary information.

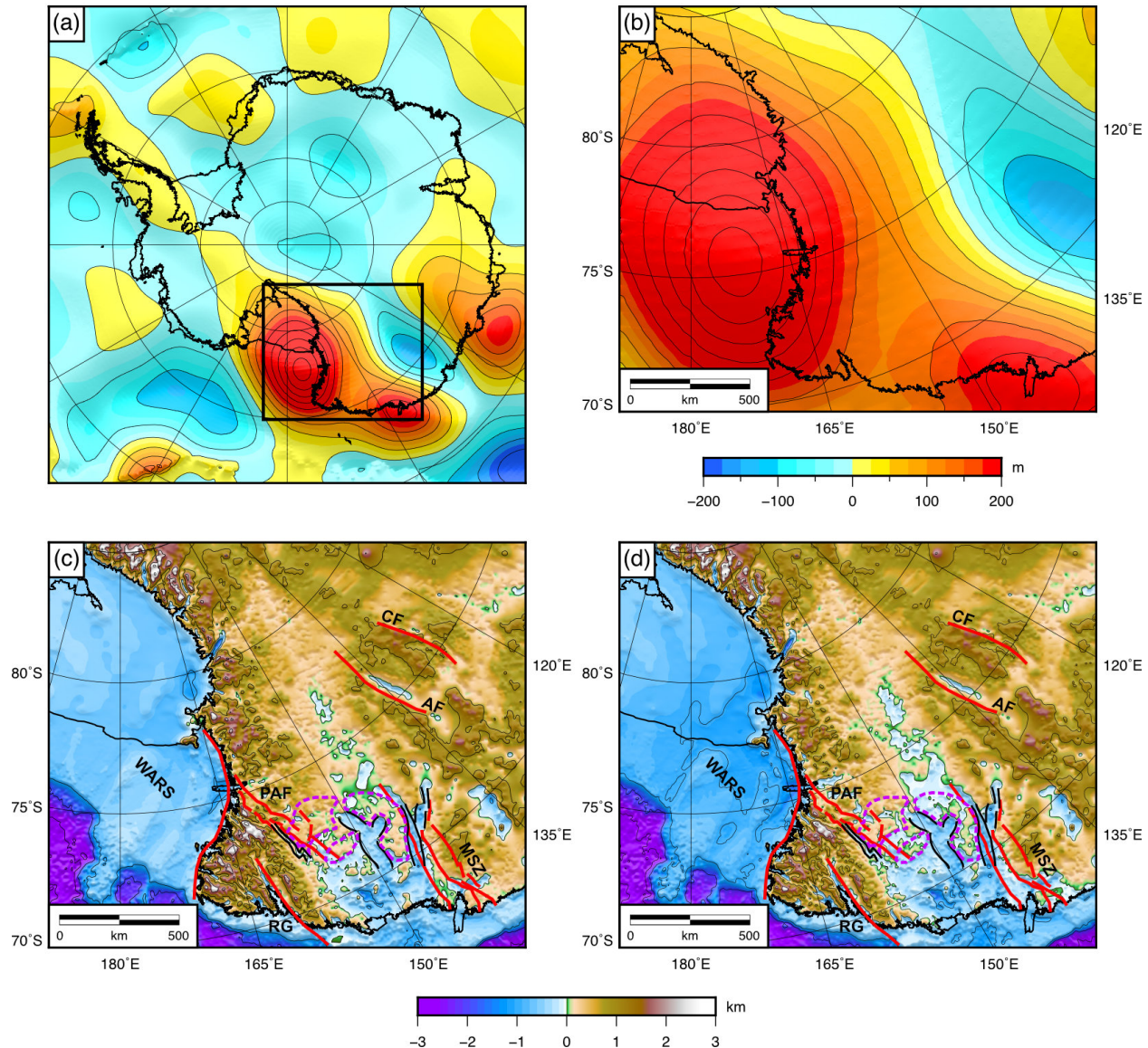


**Fig. S9.** Effect of dynamic topography change in the Wilkes Subglacial Basin. (a) Change in dynamic topography in Antarctica since 3 Ma (Austermann et al., 2015). (b) Dynamic topography change in the TAM and WSB. Contour interval is 50 meters. The northern WSB has been dynamically uplifted by ~100 m, and the TAM in Victoria Land have been uplifted by ~200 m. (c) Reconstruction of paleotopography during the mid-Pliocene without accounting for changes in dynamic topography. (d) Reconstruction of paleotopography incorporating changes in dynamic topography. Correcting for dynamic topography change results in a deeper WSB, with topography situated below sea level extending further inland. The implication is that the EAIS in this region would have experienced a larger amount of retreat than predicted if changes in dynamic topography are not included in paleotopographic reconstructions (Austermann et al., 2015). Red lines are major crustal faults (Aitken et al., 2014; Cianfarra and Salvini, 2016; Ferraccioli and Bozzo, 2003); black lines show sub-basin outlines (Ferraccioli et al., 2009); dashed magenta lines mark the extent of flat bedrock plateaus (Paxman et al., 2018). Abbreviations of major fault systems: AF = Adventure Fault; CF = Concordia Fault; MSZ = Mertz Shear Zone; PAF = Prince Albert Fault; RG = Rennick Graben; WARS = West Antarctic Rift System.